

Time-Dependent Finite-Volume Model of Thermoelectric Devices

David Yan, *Member, IEEE*, Francis P. Dawson, *Fellow, IEEE*, Mary Pugh, and Amgad A. El-Deib, *Member, IEEE*

Abstract—Thermoelectric modules are an important alternative to heat engines in the harvesting of waste heat. Electrical–thermal analogs are often employed when studying heat conduction and this approach can be extended to develop a model for thermoelectric effects. In this article, the coupled thermoelectric partial differential equations are discretized using the finite-volume method; the discretization respects the coupling between the heat sink and the thermoelectric material. The new model is especially useful when an accurate picture of transients in a thermoelectric device is required. Results from the 1-D finite-volume model are shown to agree with experimental results as well as 3-D simulations using COMSOL.

Index Terms—Finite-volume methods, modeling, thermoelectric devices, thermoelectric energy conversion, thermoelectricity.

I. INTRODUCTION

WASTE heat is produced as a byproduct in power generation, industrial processes and electrical machines. Large amounts of waste heat are produced by industry; low-grade heat (heat sources roughly under 100 °C) is also available from natural sources [1]. Recovering this heat into usable electricity would save a significant amount of resources through increasing efficiency and lowering fuel costs as well as being beneficial to the environment [2]. One prominent technology in waste heat recovery is the thermoelectric generator, which uses materials with a high thermoelectric figure of merit to convert heat to electricity [3]. Despite relatively low efficiency, their solid-state nature allows them to be used in applications where a heat engine would be impractical, such as those located in remote or hostile environments [4]. Recent experimental and application interest in thermoelectric materials has been in thin films [5], [6] and the design of microscale energy converters [7]–[10]. Modern thermoelectric devices for specialist applications are often cascaded or multi-stage [11], [12] to optimize efficiency,

meaning that the Seebeck coefficient must be modeled as having a temperature dependence. This highlights the need for accurate models to guide design and experiment.

Due to the ease with which electrical circuits can be used to study the heat equation, circuit models are commonly applied to thermoelectric problems. Examples found in the literature range from lumped equivalent circuits [13]–[15] to distributed circuits [16], [17]. Many of these are overly simplified and do not properly account for the physics of the device, including the temperature dependence of the Seebeck coefficient. The proper way to account for unmodeled physics is to discretize the partial differential equations describing the electrical and thermal characteristics of the thermoelectric device and then if required convert the series of ordinary differential equations into circuits using dependent sources, independent sources and discrete passive components. Though any partial differential equation, after discretization, can be converted into a circuit model by adding dependent sources, the main concern is that most circuit models are derived from empirical equations instead of using a first-principles approach. Additionally, many simulators cannot handle dependent sources (particularly if there is a nonlinearity), resulting in the scope of some models being limited by the capabilities of software packages.

This work starts with the partial differential equations (PDEs) for the full system: two heat equations (one for the heat source, the other for the heat sink) coupled to a pair of PDEs in the thermoelectric material (one for the temperature and one for the electric field). The PDEs are discretized using the finite-volume method, which is chosen for this work because it easily handles PDEs like (4)–(6) that involve flux terms. By taking this approach, all assumptions are known and the model can be easily related back to the governing equations. In the discretization process, one can adjust the model's accuracy and complexity by how fine a discretization is chosen and by how one approximates the boundary conditions and the transport coefficients. Furthermore, PDEs are time-dependent and the discretization yields a model that naturally contains the time-dependence of the physics through its ordinary differential equations (ODEs). An equivalent circuit model could then be created from the system of ODEs to provide a circuit that could be imported or used for visualization purposes, though creating such a model would not be necessary if only simulated results are desired.

Results of the model are computed using Matlab's ODE solver and compared to experiment and 3-D finite-element simulations. It is found that, using a 1-D model, both the transient behavior and steady-state voltage profile are accurately modeled.

Manuscript received November 27, 2012; revised February 19, 2013; accepted May 14, 2013. Date of publication June 26, 2013; date of current version January 16, 2014. Paper 2012-PEDCC-688.R1, presented at the 2012 IEEE Energy Conversion Congress and Exposition, Raleigh, NC, USA, September 15–20, and approved for publication in the IEEE TRANSACTIONS ON INDUSTRY APPLICATIONS by the Power Electronic Devices and Components Committee of the IEEE Industry Applications Society.

D. Yan, F. P. Dawson, and A. A. El-Deib are with the Department of Electrical and Computer Engineering, University of Toronto, Toronto, ON M5S 3G4, Canada (e-mail: dyan@ele.utoronto.ca; dawson@ele.utoronto.ca; amgad.eldeib@utoronto.ca).

M. Pugh is with the Department of Mathematics, University of Toronto, Toronto, ON M5S 3G4, Canada (e-mail: mpugh@math.utoronto.ca).

Color versions of one or more of the figures in this paper are available online at <http://ieeexplore.ieee.org>.

Digital Object Identifier 10.1109/TIA.2013.2271272

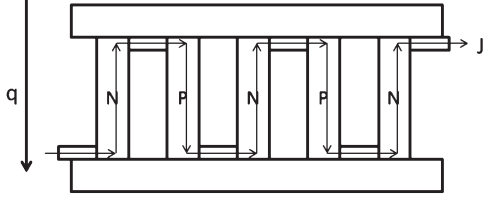


Fig. 1. Typical TE module. A commercial module may have roughly 50 couples in a square cross-sectional arrangement.

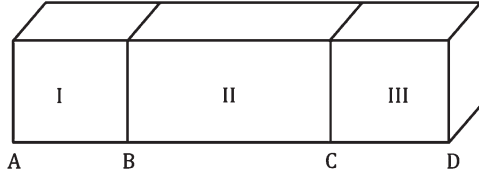


Fig. 2. Three-dimensional rectangular prism. Region I: heat source, region II: thermoelectric material, region III: heat sink.

II. FINITE-VOLUME MODEL

In the design of thermoelectric devices for power generation, optimal performance comes with having the largest thermal resistance with the smallest electrical resistance while achieving a reasonable open circuit voltage [18]. This leads to the typical “sandwich” design, with many thermocouples electrically in series and thermally in parallel, capped at either end by thermally conducting plates. A diagram of a typical thermoelectric (TE) module is shown (from a side perspective) in Fig. 1. From a modeling viewpoint, the combination of a small height with a large cross-sectional area imposes a high aspect ratio on the problem, minimizing fringing effects on the electrical and thermal fields.

For these reasons, for our model we assume no variations of temperature or the electric field in two of the three spatial dimensions, allowing the geometry to be approximated by a single slab with no-flux boundary conditions along the side walls, as shown in greater detail in the following section. We then discuss in Section II-D how the parameters in the slab model can be scaled to simulate a full many-element module, and show in Section III that this method does indeed lead to accurate results.

A. PDEs and Boundary Conditions

The geometry we will be working with is a rectangular prism of thermoelectric material capped by a heat source and sink (see Fig. 2). Regions I and III represent the heat source and sink, respectively. Region I is also referred to as the “high-side” and region III as the “low-side”. Region II represents the thermoelectric material. There is thermal and electrical insulation along the length of the prism (top, bottom, front, and back in Fig. 2). A heat flux is imposed at the leftmost end, marked “A” in the figure. An electrical current is imposed where the heat source meets the thermoelectric material, marked “B” in the figure. Electrical ground is located at the boundary marked “C” in the figure and finally, the right-most end, marked “D” in the figure is set to an ambient temperature. Taking x as the

lengthwise coordinate, the boundary conditions at A, B, C, and D are assumed to be independent of y and z .

In regions I and III the dynamics are governed by the heat equation (diffusion according to Fourier’s law)

$$\rho_I C_{vI} \frac{\partial T}{\partial t} = \nabla \cdot (k_I \nabla T) \quad (1)$$

where T is the temperature, ρ_I is the density of region I, C_{vI} is its specific heat, and k_I is the thermal conductivity. If region III is a different material, these parameters will have different values. In the thermoelectric region, region II, the dynamics are governed by

$$\rho_{II} C_{vII} \frac{\partial T}{\partial t} = \sigma \mathbf{E} \cdot \mathbf{E} - \sigma \alpha \mathbf{E} \cdot \nabla T + \nabla \cdot [(k_{II} + \sigma \alpha^2 T) \nabla T - \sigma \alpha T \mathbf{E}] \quad (2)$$

$$\frac{\partial \rho}{\partial t} = \nabla \cdot (-\sigma \mathbf{E} + \sigma \alpha \nabla T). \quad (3)$$

Here, \mathbf{E} is the electric field, ρ is the charge density, σ is the electrical conductivity, and α is the Seebeck coefficient.

With reference to Fig. 2, the boundary conditions are:

- 1) At A, $\mathbf{q} \cdot \mathbf{n} = -q_0$.
- 2) At B, $\mathbf{J} \cdot \mathbf{n} = -J_0$ and the temperature and heat flux are continuous across the interface.
- 3) At C, a voltage V_0 is imposed and the temperature and heat flux are continuous across the interface.
- 4) At D, A temperature T_{amb} is imposed.

It is assumed that the material properties are constant within each region although spatially-dependent properties could be easily handled. Also, except for the Seebeck coefficient α , the material properties are assumed to be independent of temperature and voltage. The Seebeck coefficient is assumed to be a function of temperature, $\alpha = \alpha(T)$; see Fig. 9 for an example of its temperature dependence.

B. FVM Discretization of the One Dimensional Equations

The boundary conditions at A, B, C, and D are assumed to be independent of y and z . This, combined with the no-flux boundary conditions on the lateral sides means that (1)–(3) have solutions that depend only on x and that solutions that depend on x , y , and z will converge to steady states that depend only on x . For this reason, rather than studying the fully 3-D problem given by (1)–(3), in the following we consider the 1-D reduction (described below)

$$\rho_I C_{vI} \frac{\partial T}{\partial t} = \frac{\partial}{\partial x} \left(k_I \frac{\partial T}{\partial x} \right) \quad (4)$$

$$\rho_{II} C_{vII} \frac{\partial T}{\partial t} = \sigma E^2 - \sigma \alpha E \frac{\partial T}{\partial x} + \frac{\partial}{\partial x} \left[(k_{II} + \sigma \alpha^2 T) \frac{\partial T}{\partial x} - \sigma \alpha T E \right] \quad (5)$$

$$\epsilon \frac{\partial E}{\partial t} = J_0 - \sigma E + \sigma \alpha \frac{\partial T}{\partial x} \quad (6)$$

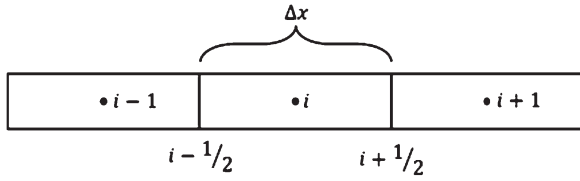


Fig. 3. $i - 1$ st, i th, and $i + 1$ st meshes. The node in the center is x_i . The boundaries are located at $x_{i-1/2}$ and $x_{i+1/2}$.

where (6) has been obtained by integrating (3) and setting the constant to J_0 and E is now the x -component of the unidirectional electric field, $\mathbf{E} = (E, 0, 0)$. The mathematics in the remainder of this section will be concerned with the numerical solution of the 1-D equations.

Each region is divided into subintervals (or meshes). For simplicity, in the following we assume that all subintervals are of the same length: each mesh is of length Δx , centered about x_i with endpoints $x_{i-1/2}$ and $x_{i+1/2}$ (see Fig. 3). Using different mesh-lengths in different regions or using nonuniform meshes within regions would lead to minor changes in the following.

Functions of x such as $T(x, t)$ and $E(x, t)$ are averaged over subintervals, replacing each function with a vector of values. For example, the i th entry of $\bar{T}(t)$ is

$$\bar{T}_i(t) := \frac{1}{\Delta x} \int_{x_{i-1/2}}^{x_{i+1/2}} T(x, t) dx. \quad (7)$$

The PDEs are averaged over subintervals as well, for example the average of the heat (1) is

$$\rho_I C_{vI} \frac{d\bar{T}_i}{dt} = \frac{1}{\Delta x} \left(k_I \frac{\partial T}{\partial x} \Big|_{x_{i+1/2}} - k_I \frac{\partial T}{\partial x} \Big|_{x_{i-1/2}} \right). \quad (8)$$

Because the material properties were assumed constant in region I there was no approximation in writing $\rho C_v dT/dt = \rho C_{vI} d\bar{T}/dt$. If they were functions of space then an approximation would be made: the average of a product would be approximated by the product of the averages. If the functions f and g are smooth enough then $\overline{fg} = \bar{f}\bar{g} + \mathcal{O}(\Delta x^2)$. Averaging the nonlinear terms in the thermoelectric (5), (6) is handled in this way.

No approximations have been made in obtaining (8). However, its right-hand side cannot be determined exactly in terms of the average \bar{T} . Instead, it is approximated via

$$k_I \frac{\partial T}{\partial x} \Big|_{x_{i+1/2}} \approx \frac{1}{\Delta x} (k_I \bar{T}_{i+1} - k_I \bar{T}_{i-1}). \quad (9)$$

Proceeding in this way, the heat (4) in regions I and III is approximated by the ODE

$$\rho_I C_{vI} \frac{d\bar{T}_i}{dt} = \frac{k_I}{\Delta x} \left[\left(\frac{\bar{T}_{i+1} - \bar{T}_i}{\Delta x} \right) - \left(\frac{\bar{T}_i - \bar{T}_{i-1}}{\Delta x} \right) \right] \quad (10)$$

and the thermoelectric (5), (6) in region II are approximated by the ODEs

$$\begin{aligned} \rho_{II} C_{vII} \frac{d\bar{T}_i}{dt} = & \sigma \bar{E}_i^2 - \sigma \bar{\alpha}_i \bar{E}_i \frac{\bar{T}_{i+1} - \bar{T}_{i-1}}{2\Delta x} \\ & + \frac{k_{II}}{\Delta x} \left[\frac{\bar{T}_{i+1} - 2\bar{T}_i + \bar{T}_{i-1}}{\Delta x} \right] \\ & + \frac{\sigma \bar{\alpha}_i^2}{\Delta x} \left[\frac{\bar{T}_{i+1} + \bar{T}_i}{2} \frac{\bar{T}_{i+1} - \bar{T}_i}{\Delta x} \right. \\ & \quad \left. - \frac{\bar{T}_i + \bar{T}_{i-1}}{2} \frac{\bar{T}_i - \bar{T}_{i-1}}{\Delta x} \right] \\ & - \frac{\sigma \bar{\alpha}_i}{\Delta x} \left[\frac{\bar{T}_{i+1} + \bar{T}_i}{2} \frac{\bar{E}_{i+1} + \bar{E}_i}{2} \right. \\ & \quad \left. - \frac{\bar{T}_i + \bar{T}_{i-1}}{2} \frac{\bar{E}_i + \bar{E}_{i-1}}{2} \right] \quad (11) \end{aligned}$$

$$\epsilon \frac{d\bar{E}_i}{dt} = J_0 - \sigma \bar{E}_i + \sigma \bar{\alpha}_i \frac{\bar{T}_{i+1} - \bar{T}_{i-1}}{2\Delta x}. \quad (12)$$

Above, $\bar{\alpha}_i$ is shorthand for $\alpha(\bar{T}_i)$. Because the mesh is uniform, the approximate (10)–(12) are second-order accurate, $\mathcal{O}(\Delta x^2)$, if the solutions of the PDEs have bounded third derivatives.

If regions I, II, and III have been divided into N_I , N_{II} , and N_{III} subintervals of length Δx , respectively, the finite-volume discretization yields a system of $N_I + 2N_{II} + N_{III}$ ODEs. As discussed in the next section, this system of ODEs is supplemented by two more ODEs in order to discretize the boundary conditions at the interfaces B and C correctly.

C. Discretizing the Boundary Conditions

1) *Boundary Conditions at A and D:* The boundary conditions at the ends, A and D (see Fig. 2) are straightforward. At A, a heat flux is imposed: $-k(\partial T/\partial x) = q_0$. If $x_{i-1/2} = A$ then the heat flux at $x_{i-1/2}$ in (8) is simply q_0 . This leads to the ODE

$$\rho_I C_{vI} \frac{d\bar{T}_i}{dt} = \frac{k_I}{\Delta x} \left[\left(\frac{\bar{T}_{i+1} - \bar{T}_i}{\Delta x} \right) - q_0 \right] \quad (13)$$

for that subinterval. Similarly, if $x_{i+1/2} = D$ then the temperature T_{amb} is the temperature at $x_{i+1/2}$; this is used in approximating the heat flux at $x_{i+1/2}$ in (8), leading to

$$\rho_{III} C_{vIII} \frac{d\bar{T}_i}{dt} = \frac{k_{III}}{\Delta x} \left[\frac{T_{\text{amb}} - \bar{T}_i}{\Delta x/2} - \frac{\bar{T}_i - \bar{T}_{i-1}}{\Delta x} \right]. \quad (14)$$

2) *Example of Boundary Conditions at an Interface:* Before addressing the boundary conditions at B and C, let us examine the simpler case of the heat equation across an interface at which the thermal resistance changes. At the interface, the temperature and heat flux are continuous. In Fig. 4, there is an interface at $x_{i-1/2}$; the thermal resistance in the interval to the left is k_I and is k_{II} in the interval to the right.

The heat flux is continuous at $x_{i-1/2}$, hence,

$$\left(k \frac{\partial T}{\partial x} \right)_I = \left(k \frac{\partial T}{\partial x} \right)_{II} \quad (15)$$

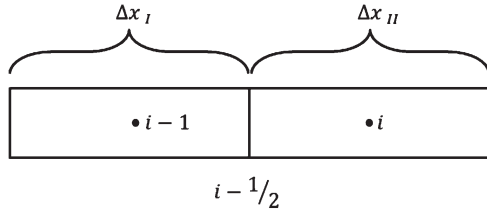


Fig. 4. Material to the left has length Δx_I and has thermal resistance k_I ; the material to the right has length Δx_{II} and thermal resistance k_{II} . The interface is located at $x_{i-1/2}$.

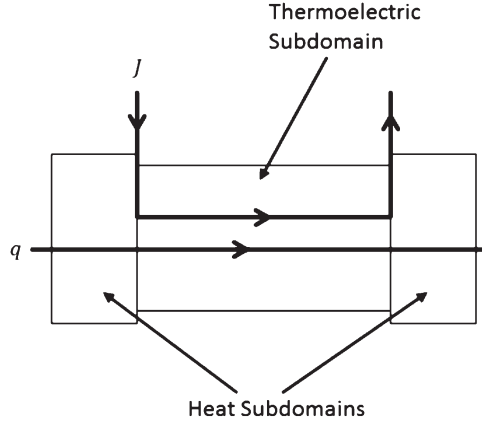


Fig. 5. Paths for the electrical and heat fluxes.

where the I subscript indicates the limiting value as x increases to $x_{i-1/2}$; the II subscript indicates the limit from the other side. Recalling that \bar{T}_{i-1} is the average temperature over the interval to the left and \bar{T}_i is the average over the interval to the right, the flux continuity at the discretized level is

$$k_I \frac{T_{I-1/2} - \bar{T}_{i-1}}{\Delta x_I/2} = k_{II} \frac{\bar{T}_i - T_{i-1/2}}{\Delta x_{II}/2} \quad (16)$$

where $T_{i-1/2}$ is the temperature at $x_{i-1/2}$. The continuity of the temperature at $x_{i-1/2}$ was implicit when $T_{i-1/2}$ was used in (16) to represent the both the limit from the left and the limit from the right. The temperature at the interface is determined by the continuity of flux; solving (16) yields

$$T_{i-1/2} = \frac{\frac{\Delta x_I}{k_I} \bar{T}_i + \frac{\Delta x_{II}}{k_{II}} \bar{T}_{i-1}}{\frac{\Delta x_I}{k_I} + \frac{\Delta x_{II}}{k_{II}}}. \quad (17)$$

This approximation is well known to electrical engineers as the one made in circuit theory for resistor dividers. Using (17) in (16) yields an approximation of the flux at $x_{i-1/2}$ in terms of the average temperatures on either side of the interface

$$\left(k \frac{\partial T}{\partial x} \right)_I = \left(k \frac{\partial T}{\partial x} \right)_{II} \approx \frac{2(\bar{T}_i - \bar{T}_{i-1})}{\frac{\Delta x_I}{k_I} + \frac{\Delta x_{II}}{k_{II}}}. \quad (18)$$

The expression (18) can then be used in any ODE that requires the heat flux at $x_{i-1/2}$. Approximating the heat flux in a different way than in (16) would have led to a different formula for $T_{i-1/2}$ and a different expression for (18).

3) *Boundary Conditions at the Interfaces B and C:* The paths for the electrical and heat fluxes are shown in Fig. 5. In

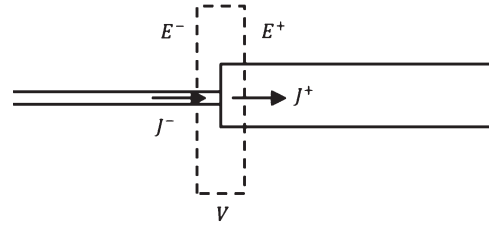


Fig. 6. Dashed line denotes a Gaussian Surface, ∂V , enclosing the interface B. The electric field and current are approximately unidirectional with x -components E^- and J^- on the “wire” side of B and components E^+ and J^+ on the thermoelectric material side of B.

a real thermoelectric device, the electrical current would enter and leave via soldered wires while the heat flux flows through the top and bottom plates. Regions I and III represent the materials in the path of the heat flux and are included in the model because they contribute significantly to the transient response, while the electrical domains outside of the thermoelectric material are not modeled because they contribute very little. This presents a unique difficulty because in the model the interface is between a pair of PDEs for T and E (5), (6) that hold in a region in which there are electrical material properties (region II) and a single PDE for T , (4), that holds in a region in which the electrical material properties are technically undefined. For this reason, in the discretization rather than choosing to have a subinterval that straddles the interface we take the interface to be flanked by two subintervals. Each flanking subinterval is fully within region I/III or region II and it is clear what material properties to use and which PDEs to average. We focus on the interface at B; the interface at C is handled in a similar manner. From the PDEs (4) and (5) the continuity of heat flux at the interface B is

$$\left(k_I \frac{\partial T}{\partial x} \right)_I = \left((k_{II} + \sigma \alpha^2 T) \frac{\partial T}{\partial x} - \sigma \alpha T E \right)_{II}. \quad (19)$$

If the electric field at B were known then the discretization of (19) would yield an equation that could be solved for the temperature at B, ultimately leading to an expression for the heat flux at the interface in terms of the average temperatures on either side and the electric field at the interface.

This raises the question of how to approximate the electric field at the interface B when the electrical boundary condition at B is that a current, J_0 , is imposed. Fig. 6 shows a Gaussian surface enclosing the interface B. The left side is a wire which we approximate as having zero electric field $\mathbf{E} = (0, 0, 0)$ and a forcing current density of $\mathbf{J} = (J_0, 0, 0)$. The right side is the thermoelectric material which we approximate as having a unidirectional electric field $\mathbf{E} = (E^+, 0, 0)$ and current density $\mathbf{J} = (J^+, 0, 0)$.

The charge conservation equation and Gauss’s law are

$$\nabla \cdot \mathbf{J} + \frac{\partial \rho}{\partial t} = 0, \quad \nabla \cdot \mathbf{E} = \frac{\rho}{\epsilon} \quad (20)$$

where ρ is the electric charge density; the free charge density is assumed to equal the charge density. Taking the integral of

over the volume V shown in Fig. 6 and using the Divergence theorem yields

$$\int_{\partial V} \mathbf{J} \cdot \mathbf{n} dS + \frac{d}{dt} \int_V \rho dV = 0, \epsilon \int_{\partial V} \mathbf{E} \cdot \mathbf{n} dS = \int_V \rho dV \quad (21)$$

where \mathbf{n} is the outward unit normal to the surface ∂V . Combining the two equations yields

$$\int_{\partial V} \mathbf{J} \cdot \mathbf{n} dS + \epsilon \int_{\partial V} \frac{\partial \mathbf{E}}{\partial t} \cdot \mathbf{n} dS = 0. \quad (22)$$

By symmetry, the contributions to the surface integrals from the top and bottom of ∂V cancel. Taking the sides of ∂V to the interface, and using that \mathbf{J} and \mathbf{E} depend on x and t only, (22) becomes

$$J^+ - J^- + \epsilon \left(\frac{dE^+}{dt} - \frac{dE^-}{dt} \right) = 0. \quad (23)$$

Because $E^- = 0$, $J^- = J_0$, and $J^+ = \sigma E^+ - \sigma \alpha (\partial T / \partial x)$, (23) becomes

$$\epsilon \frac{dE^+}{dt} = J_0 - \sigma E^+ + \sigma \alpha \frac{\partial T}{\partial x}. \quad (24)$$

Note that because $E^+(t) = E(B, t)$, this is the limit of the PDE (6) as x approaches B from within the thermoelectric material.

At the PDE level, the heat flux balance is (19) where $E_{II}(t)$ is the solution of (24). Discretizing these, the temperature at the interface, $T_{i-1/2}$, solves

$$\frac{T_{i-1/2} - \bar{T}_{i-1}}{\Delta x_I / 2k_I} = \frac{\bar{T}_i - T_{i-1/2}}{\Delta x_{II} / 2k_{II}} - \sigma \bar{\alpha}_i \bar{T}_i \frac{\bar{T}_i - T_{i-1/2}}{\Delta x_{II} / 2} - \sigma \bar{\alpha}_i \bar{T}_i E_{i-1/2} \quad (25)$$

where $E_{i-1/2}$ is a solution of

$$\epsilon \frac{dE_{i-1/2}}{dt} = J_0 - \sigma E_{i-1/2} + \sigma \bar{\alpha}_i \frac{\bar{T}_i - T_{i-1/2}}{\Delta x / 2}. \quad (26)$$

Solving (25) for $T_{i-1/2}$ yields

$$T_{i-1/2} = \left(\frac{\Delta x_{II} \bar{T}_{i-1}}{k_{II}} + \frac{\Delta x_I \bar{T}_i}{k_I} - \frac{\sigma \bar{\alpha}_i^2 \Delta x_I \bar{T}_i}{k_I k_{II}} - \frac{\sigma \bar{\alpha}_i \Delta x_I \Delta x_{II} \bar{T}_i E_{i-1/2}}{2k_I k_{II}} \right) / \left(\frac{\Delta x_I}{k_I} + \frac{\Delta x_{II}}{k_{II}} - \frac{\sigma \bar{\alpha}_i^2 \Delta x_I \bar{T}_i}{k_I k_{II}} \right). \quad (27)$$

Substituting (27) into the ODE (26) for $E_{i-1/2}$ results in an ODE of the form

$$\epsilon \frac{dE_{i-1/2}}{dt} = J_0 + a - bE_{i-1/2} \quad (28)$$

where a depends on \bar{T}_{i-1} , \bar{T}_i , the mesh widths, and the material properties; b depends on \bar{T}_i , the mesh widths, and the material properties. This ODE is solved along with the ODES (10)–(12).

Substituting (27) into (25), the heat flux at B is approximately

$$2 \left(\bar{T}_i - \bar{T}_{i-1} - \frac{\sigma \bar{\alpha}_i^2}{k_{II}} \bar{T}_i (\bar{T}_i - \bar{T}_{i-1}) - \frac{\sigma \bar{\alpha}_i \Delta x_{II} \bar{T}_i E_{i-1/2}}{2k_{II}} \right) / \left(\frac{\Delta x_{II}}{k_{II}} + \frac{\Delta x_I}{k_I} - \frac{\sigma \bar{\alpha}_i^2 \Delta x_I \bar{T}_i}{k_I k_{II}} \right). \quad (29)$$

This expression is used when discretizing the heat (4) in region I for the subinterval to the left of B and when discretizing the thermoelectric (5) in region II for the subinterval to the right of B.

If there is no electrical conductivity ($\sigma = 0$) or if the Seebeck coefficient vanishes ($\alpha = 0$) then the heat flux at B (29) reduces to the flux (18), as expected.

Something should be said about why one would want to use the more complicated expression (29) for the heat flux rather than choosing to ignore the additional thermoelectric terms and use the simpler expression (18). Using (18) would mean that one is effectively introducing heat flux at the interface B which would not be there naturally. To see this, one calculates the difference between (29) and (18); if this difference goes to zero as Δx goes to zero then using either formula would be fine in the limit. If the difference does not go to zero then using the heat flux given by (18) is inconsistent with the PDEs in the bulk and leads to convergence problems for the numerical simulation. In the case that $\Delta x_I = \Delta x_{II} = \Delta x$, subtracting (18) from (29) yields

$$\text{err} \approx - \frac{\sigma \bar{\alpha}_i k_I (2\bar{\alpha}_i k_{II} M + E_{i+1/2} (k_I + k_{II}))}{(k_I + k_{II})(k_I + k_{II} - \sigma \bar{\alpha}_i^2 \bar{T}_i)} \bar{T}_i. \quad (30)$$

Above, the approximation $\bar{T}_i - \bar{T}_{i-1} \approx M \Delta x$ was made where $M = [(\partial T / \partial x)_r + (\partial T / \partial x)_l] / 2$. As $\Delta x \rightarrow 0$, the error (30) will tend to the same expression but with $\bar{\alpha}_i$ replaced by $\alpha(T(B))$ and \bar{T}_i replaced by $T(B)$. Because this limit is nonzero, using (18) would lead to convergence problems.

We note that when discretizing the flux balance (19) to find the (25), we chose to evaluate the coefficients at x_i rather than at $x_{i-1/2} = B$. This yielded in an easily-solved linear equation for $T_{i-1/2}$. Had the coefficients been evaluated at $x_{i-1/2}$ instead then this would have resulted in a nonlinear equation for $T_{i-1/2}$ which can be explicitly solved (if $\alpha(T)$ near \bar{T}_i is approximated by a linear function). The difference caused by using a nonlinear equation for $T_{i-1/2}$ was tested using the code and found to be negligible.

In the experiments, the boundary condition at the interface C is that the voltage equals V_0 . This boundary condition only appears if one spatially integrates the computed electric field to construct the potential. In the model, the boundary condition used is that the current at the interface C is also J_0 ; using this and the continuity of temperature and heat flux results in a second ODE of the form (28) where the ODE's coefficients involve the temperature averaged over the two subintervals flanking C. When using formula (27) to find this ODE, I is replaced by III and the i and $i-1$ indices are interchanged. The same changes are made to the formula for the heat flux (29) before using it to discretize (4) and (5) for the two subintervals flanking C.

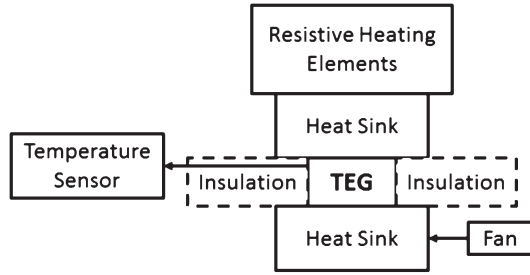


Fig. 7. Block diagram of experiment.

The FVM discretization described here could equally well be done for the 3-D system (1)–(3). Of course, the 1-D model is easier to code up, faster to compute, and the solutions are easier to visualize.

D. Scaling

The model developed so far in this paper has been for a single slab of thermoelectric material. As discussed in Section II, in nearly all applications more than one piece of material will be connected thermally in parallel and electrically in series. Therefore, we would like to relate a 3-D module of many individual thermoelectric PN couples to our 1-D model. In such a model it does not make sense to have a unified length and cross-sectional area as the electrical and heat fluxes “see” different geometries. A helpful method of dealing with this is to recast the existing equations in terms of resistances and capacitances instead of conductivities and capacities, in which case the material property, length and cross-sectional area are all lumped into a single bulk property independent of geometry. This way, any thermoelectric module with cross-sectional symmetry can be approximated as a 1-D problem with equivalent resistances and capacitances. Examples of the discretized, recast equations are given in Section III-B.

This leaves the problem of scaling the Seebeck coefficient α . As shown in Fig. 6, electrical current flows in the same direction as the heat flux in the P-type semiconductor and against the heat flux in the N-type semiconductor to produce a positive voltage difference. Since in a 1-D model we are only allowed a single value for α , the logical choice is to pick $\alpha = M(\alpha_p - \alpha_n)$ where M is the number of PN couples in the device. $\alpha(T)$ would then represent the temperature dependence of a PN thermocouple in this particular arrangement rather than a single material.

III. COMPUTATIONAL AND EXPERIMENTAL RESULTS

A. Experimental Setup

Figs. 7 and 8 show the experimental arrangement. With reference to Fig. 8, the experimental apparatus consists of: two power resistors (5) connected electrically in parallel to supply a constant heat flux to the hot side of a commercial thermoelectric Peltier cooler (2), and a heat sink (1) and fan (4) to remove heat from the cold side. A hollow oven brick (6) is placed over the heating elements and polyurethane foam insulation (3) is placed beside the thermoelectric module to provide thermal insulation. This design ensures that the amount

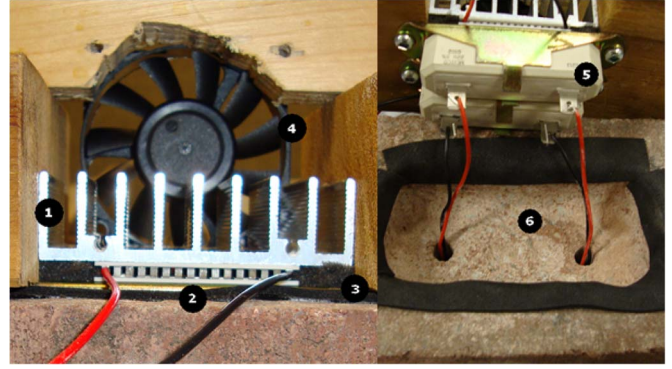


Fig. 8. Photograph of experimental apparatus. 1. Cold side heat sink 2. Thermoelectric module 3. Insulation 4. Cold side fan 5. Hot side heating elements 6. Hot side insulating brick.

TABLE I
MATERIAL PROPERTIES

Component	Material	Mass (g)	$C_p \frac{kJ}{kgK}$	$C_{th} \frac{J}{K}$
Resistors	Steatite Ceramic	72.0 (x2)	0.9 [20]	130
TE Module	Bi_2Te_3 & Ceramic	19.0		20
Heat Sink	Aluminum	36.5	0.9	33

of heat transferred through the brick is minimal since the brick is a good thermal insulator and the gap between the device and brick is small so there are no convection cells removing the heat. This makes the no-heat-flux (adiabatic) boundary condition on the side walls a valid assumption when comparing results. The experimental apparatus is similar to one used in a recent characterization experiment (refer to [19]). Using this test apparatus, measurements were performed to determine the Seebeck coefficient and bulk material properties.

Heat capacitances were measured by weighing each component and multiplying their mass by their specific heat capacities. The measured values are given in Table I. The approximation $C_p \approx C_v$ was made. Since no accurate value could be used for the heat capacity of the TE module, it was treated as a free parameter and chosen to fit the data.

The thermal resistances were measured by imposing a heat flux and then measuring the temperatures at the interfaces between the components. This yielded $R_{th} = 0.1$ K/W for the resistors, $R_{th} = 2$ K/W for the thermoelectric module, and $R_{th} = 0.8$ K/W for the heat sink. The electrical resistance of the thermoelectric module was measured using an ohmmeter and found to be $R_e = 4.4 \Omega$ ([19] gives a value of $3.88 \pm 0.13 \Omega$ for a similar module). For the electrical capacitance, an arbitrarily chosen small value was taken: $C_e = 5$ mF.

The Seebeck coefficient, $\alpha(T)$, was determined by measuring temperature differences across the thermoelectric device and their corresponding open circuit voltage. Values for $\alpha(T)$ were obtained between 307 K and 344 K and approximated as constant outside of this temperature range. Fig. 9 presents $\alpha(T)$ with the data between 307 K and 344 K interpolated using third-order Lagrange polynomial approximation.

B. Time-Dependent Solutions

The experimental measurements yield bulk properties of the components. As mentioned in Section II and II-D, the

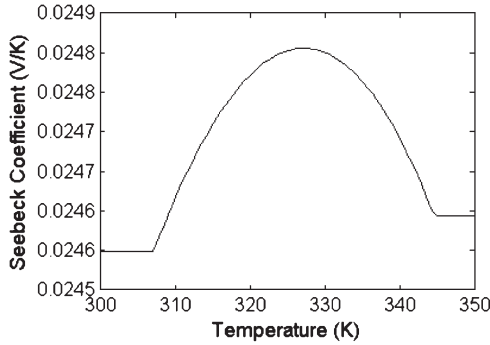


Fig. 9. Seebeck coefficient from experimental measurements.

experimental apparatus is not a simple prism like Fig. 2 although the model is approximating it as such. Reducing the bulk properties to material properties such as resistivities would require knowing the cross-section areas of all the components. Rather than doing this, we consider slices of the components with each slice linked to the next. For example, if the heat sink is approximated by N_I slices then the thermal resistance of each slice will be $\Delta C_{th} := C_{th}/N_I$.

This approach requires rewriting the ODEs (10)–(12), (26) in terms of bulk quantities such as resistances and capacitances. For example, (11), (12) become

$$\begin{aligned} \Delta C_{th} \frac{\partial \bar{T}_i}{\partial t} = & \frac{\bar{W}_i^2}{\Delta R_e} - \bar{\alpha}_i \frac{\bar{W}_i}{\Delta R_e} \frac{\bar{T}_{i+1} - \bar{T}_{i-1}}{2} \\ & + \frac{1}{\Delta R_{th}} (\bar{T}_{i+1} - 2\bar{T}_i + \bar{T}_{i-1}) \\ & + \frac{\bar{\alpha}_i^2}{2\Delta R_e} (\bar{T}_{i+1}^2 - 2\bar{T}_i^2 + \bar{T}_{i-1}^2) \\ & - \frac{\bar{\alpha}_i}{4\Delta R_e} [(\bar{T}_{i+1} + \bar{T}_i)(\bar{W}_{i+1} + \bar{W}_i) \\ & \quad - (\bar{T}_i + \bar{T}_{i-1})(\bar{W}_i + \bar{W}_{i-1})] \end{aligned} \quad (31)$$

$$\Delta C_e \frac{\partial \bar{W}_i}{\partial t} = I_0 - \frac{\bar{W}_i}{\Delta R_e} + \bar{\alpha}_i \frac{\bar{T}_{i+1} - \bar{T}_{i-1}}{2\Delta R_e} \quad (32)$$

where $\Delta C_{th} = C_{th}/N_{II} = \mathcal{A}\Delta x\rho C_v$ is the thermal capacitance, $\Delta R_{th} = R_{th}/N_{II} = \Delta x/(k\mathcal{A})$ is the thermal resistance, $\Delta R_e = R_e/N_{II} = \Delta x/(\sigma\mathcal{A})$ is the electrical resistance, $\Delta C_e = N_{II}C_e = \mathcal{A}\epsilon/\Delta x$ is the electrical capacitance, and $I_0 = \mathcal{A}J_0$ is the current. \mathcal{A} is the cross-sectional area and Δx is the thickness of the slice. $\bar{W}_i = \bar{E}_i\Delta x$ is used in place of \bar{E}_i , and can be thought of as the voltage difference across each subinterval.

The time-dependent voltage was obtained by taking the apparatus at room temperature (293K), applying an input power of 20 W and periodically measuring the open-circuit voltage. Fig. 10 presents the experimentally measured voltage as a function of time.

Matlab's ode23 solver (an explicit Runge–Kutta method) was then used to solve the (re-formulated) system of $N_I + N_{II} + N_{III} + 2$ ODEs (10), (26) and (31), (32) using the coefficients used in the code are those given in Section III-A. The initial data was $\bar{T}_i = 293$ and $\bar{W}_i = 0$ for all i and $N_I = N_{II} = N_{III} = 20$. Fig. 10 plots the $\sum \bar{W}_i$, which approximates the voltage across the thermoelectric material, as a function of time.

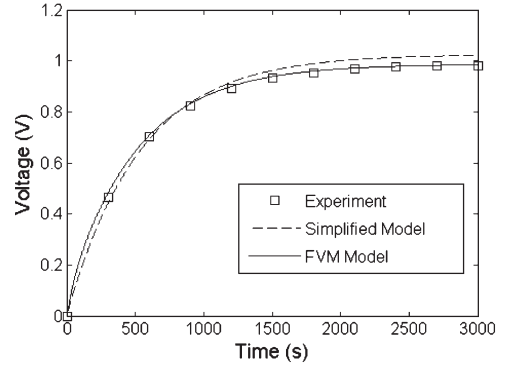


Fig. 10. Open circuit voltage versus time.

The experiment and simulation are compared with the results of a very simplified model. In this simple model, the three regions are treated as bulk objects ($N_I = N_{II} = N_{III} = 1$) that are thermally coupled but have no thermoelectric properties: the ODE (10) in regions I and III, the ODE (11) with $\sigma = 0$ in region II, and the boundary conditions (16) at the interfaces B and C. At each moment in time, the temperatures at B and C are constructed using (17) and their difference is multiplied by α_{av} to produce an approximate voltage across the thermoelectric region as a function of time (see Fig. 10). Here, α_{av} is the average value of $\alpha(T)$ on over the interval of measurements ([307, 344]) (see Fig. 9).

Fig. 10 shows excellent agreement between the experiment and the 1-D finite-volume model; admittedly the coefficients used in the finite-volume model did come from the experimental apparatus rather than from CRC manuals, nevertheless the experimental apparatus has more complicated geometry than a prism like that shown in Fig. 2. The simple model also does well in the early part of the dynamics, due to the behavior at small t being dominated by the heat capacity of the heat source and sink. However, its limiting, steady state behavior disagrees with with the experiments and the finite-volume model. This is not just that the simple model uses a constant for the Seebeck coefficient, it's also that the steady state of the simple model is consistent with a piece-wise linear solution; a linear-in- x temperature cannot be part of a steady state solution of the TE equations.

C. Steady-State Solutions

As a further test of the finite-volume model, we compared it to a 3-D finite element simulation of the thermoelectric slab shown in Fig. 2 using COMSOL. COMSOL computes steady states directly; to find steady states of the finite-volume model we computed a solution of the initial value problem to a large time and used that.

The COMSOL simulation (based on [21]) was for a prism (see Fig. 2). The heat source and sink were copper and the thermoelectric material was bismuth telluride. The experimentally measured Seebeck coefficient for bismuth telluride (see Fig. 9) is not that far from constant: the maximum (.0248) is less than 0.5% larger than the average (0.0247). This produced a nearly linear voltage and temperature profile for the steady-state solution, making it difficult to evaluate whether the

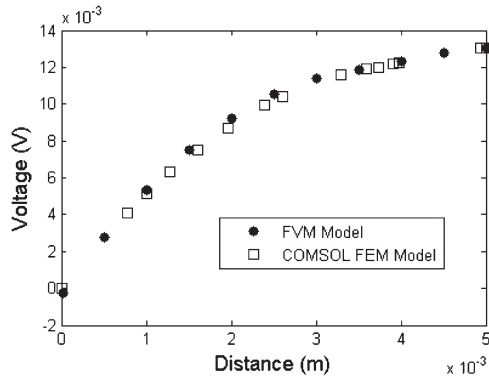


Fig. 11. Comparison between the 1-D finite-volume model and 3-D COMSOL results for the steady-state voltage profile within the thermoelectric material.

finite-volume model is accurately portraying the multiphysics. Thus, for testing purposes we used an artificial $\alpha(T)$ which is linear over the range $T = (305, 345)$:

$$\alpha(T) = 2 \times 10^{-5}(T - 300) \text{ V/K}. \quad (33)$$

For this choice, the maximum value $\alpha(345) = 0.0009$ is 80% larger than the average value $\alpha(325) = 0.0005$.

For a steady-state simulation, the density and specific heat of copper are not needed [see (1)] but the thermal conductivity $k_I = 400 \text{ W/(mK)}$ is needed for the flux boundary conditions [see (19)]. For the bismuth telluride steady state one needs $\sigma = 1.6 \text{ S/m}$, $k_{II} = 1.5 \text{ W/(mK)}$, $\alpha(T)$ [see (33)], and the imposed current $J_0 = 0$. These values were used in COMSOL to compute the steady state; the voltage profile within the thermoelectric material is shown in Fig. 11. The material properties and volumes were then used to define bulk properties that were used in the finite-volume model; the large-time voltage profile is shown in Fig. 11. As can be seen, there is an almost exact match between the two methods, thus validating our approach.

IV. CONCLUSION

To address limitations of current thermoelectric models such as not being time-dependent or not having temperature-dependent transport coefficients, we have developed a 1-D finite-volume model for thermoelectric devices. A 1-D approach was taken due to the symmetries present in most applications involving thermoelectric materials and the geometry was divided into three regions: the high side heat exchanger, the thermoelectric material and the low side heat exchanger. The PDEs for the three regions were discretized using a center-differencing finite-volume method. Particular attention was paid to the internal boundaries where heat flux balance was enforced in order to obtain the correct expressions for the boundary temperatures and voltages.

The finite-volume model developed here has three important advantages over existing models. First, the ODEs in the model were derived directly from the governing PDEs. As a result, the modeling equations can all be traced back to the original physics and proper electro-thermal coupling is ensured. Secondly, the temperature dependence of the transport coefficients

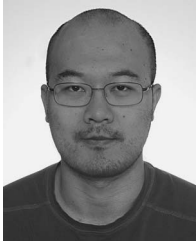
and the time dependence of the temperature and voltage are naturally incorporated into the model from the beginning. Finally, the model includes the high and low side heat sinks, which are key to the dynamics, and properly treats the heat flux balance at the boundaries.

Using MATLAB, results from the finite-volume model were compared to experiments and to results of a 3-D finite-element model implemented with COMSOL. The results using a 1-D analysis are in agreement with a 3-D result, indicating that for conventional TE designs it is not necessary to consider a 3-D formulation.

REFERENCES

- [1] A. W. Crook, *Profiting From Low-Grade Waste Heat*. London, U.K.: Inst. Elect. Eng., 1994.
- [2] D. M. Rowe, *CRC Handbook of Thermoelectrics*. Danvers, MA, USA: CRC Press, 1995.
- [3] A. Harb, "Energy harvesting: State-of-the-art," *Renew. Energy*, vol. 36, no. 10, pp. 2641–2654, Oct. 2011.
- [4] R. O'Brien, R. Ambrosi, N. Bannister, S. Howe, and H. Atkinson, "Safe radioisotope thermoelectric generators and heat sources for space applications," *J. Nucl. Mater.*, vol. 393, no. 3, pp. 504–506, Jul. 2008.
- [5] H. Yousef, K. Hjort, and M. Lindeberg, "Vertical thermopiles embedded in a polyimide-based flexible printed circuit board," *J. Microelectromech. Syst.*, vol. 16, no. 6, pp. 1341–1348, Dec. 2007.
- [6] A. Yamamoto, H. Hagino, Y. Hashimoto, and K. Miyazaki, "The effects of thermoelectric film thickness on performance of in-plane thermoelectric modules," *J. Electron. Mater.*, vol. 41, no. 6, pp. 1799–1804, Jun. 2012.
- [7] Z. Wang, V. Leonov, P. Fiorini, and C. V. Hoof, "Realization of a wearable miniaturized thermoelectric generator for human body applications," *Sens. Actuator A, Phys.*, vol. 156, no. 1, pp. 95–102, Nov. 2009.
- [8] J. P. Carmo, L. M. Gonçalves, and J. H. Correia, "Thermoelectric microconverter for energy harvesting systems," *IEEE Trans. Ind. Electron.*, vol. 57, no. 3, pp. 861–867, Mar. 2010.
- [9] D. D. L. Wijngaards and R. F. Wolffenbuttel, "Thermoelectric characterization of APCVD PolySi_{0.7}Ge_{0.3} for IC-compatible fabrication of integrated lateral peltier elements," *IEEE Trans. Electron Devices*, vol. 52, no. 5, pp. 1014–1025, May 2005.
- [10] N. B. Crane, P. Mishra, J. L. Murray, Jr., and G. S. Nolas, "Self-assembly for integration of microscale thermoelectric coolers," *J. Electron. Mater.*, vol. 38, no. 7, pp. 1252–1256, Jul. 2009.
- [11] G. E. Bulman, E. Siivola, R. Wiitala, R. Venkatasubramian, M. Acree, and N. Ritz, "Three-stage thin-film superlattice thermoelectric multistage microcooler with a ΔT_{max} of 102 K," *J. Electron. Mater.*, vol. 38, no. 7, pp. 1510–1515, Jul. 2009.
- [12] R. Yang, G. Chen, G. J. Snyder, and J.-P. Fleurial, "Multistage thermoelectric microcoolers," *J. Appl. Phys.*, vol. 95, no. 12, pp. 8226–8232, Jun. 2004.
- [13] J. A. Chavez, J. A. Ortega, J. Salazar, A. Turo, and M. J. Garcia, "SPICE model of thermoelectric elements including thermal effects," in *Proc. IEEE Instrum. Meas. Conf.*, 2000, vol. 2, pp. 1019–1023.
- [14] S. Lineykin and S. Ben-Yaakov, "Analysis of thermoelectric coolers by a SPICE-compatible equivalent circuit model," *IEEE Power Electron. Lett.*, vol. 3, no. 2, pp. 63–66, Jun. 2005.
- [15] D. Wijngaards, E. Cretu, S. Kong, and R. Wolffenbuttel, "Modelling of integrated peltier elements," in *Proc. Int. Conf. Model. Simul. Microsyst.*, 2000, pp. 582–588.
- [16] M. Chen, L. A. Rosendahl, I. Bach, T. Condra, and J. K. Pedersen, "Transient behavior study of thermoelectric generators through an electro-thermal model using SPICE," in *Proc. 25th Int. Conf. Thermoelectrics*, 2006, pp. 214–219.
- [17] D. Mitrani, J. Salazar, A. Turo, M. Garcia, and J. Chavez, "One-dimensional modeling of TE devices considering temperature-dependent parameters using SPICE," *Microelectron. J.*, vol. 40, no. 9, pp. 1398–1405, Sep. 2009.
- [18] S. A. Omer and D. G. Infield, "Design optimization of thermoelectric devices for solar power generation," *Solar Energy Mater. Sol. Cells*, vol. 53, no. 1/2, pp. 67–82, May 1998.
- [19] J. P. Carmo, J. Antunes, M. F. Silva, J. F. Ribeiro, L. M. Goncalves, and J. H. Correia, "Characterization of thermoelectric generators by measuring the load-dependence behavior," *Measurement*, vol. 44, no. 10, pp. 2194–2199, Dec. 2011.

- [20] W. Martienssen and H. Warlimont, *Springer Handbook of Condensed Matter and Materials Data*, vol. 1. Berlin, Germany: Springer-Verlag, 2005.
- [21] D. Ebling, M. Jaegle, M. Bartel, A. Jacquot, and H. Böttner, "Multiphysics simulation of thermoelectric systems for comparison with experimental device performance," *J. Electron. Mater.*, vol. 38, no. 7, pp. 1456–1461, Jul. 2009.



David Yan (S'02–M'09) received the B.A.Sc. and M.A.Sc. degrees in engineering science and electrical engineering, respectively, from the University of Toronto, Toronto, ON, Canada, in 2009 and 2011, respectively. For his master's thesis, he created a time-dependent finite-volume model for thermoelectrics. He is currently working toward the Ph.D. degree at the University of Toronto, developing mathematical models and simulation tools for electrochemical devices.



Francis P. Dawson (S'86–M'87–F'09) received the B.Sc. degree in physics and the B.A.Sc., M.A.Sc., and Ph.D. degrees in electrical engineering from the University of Toronto, Toronto, ON, Canada, in 1978, 1982, 1985, and 1988, respectively.

He worked as a Process Control Engineer in the pulp and paper, rubber, and textile industries during the period 1978–1980. From 1982 to 1984, he acted as a Consultant on various projects. Development areas included high-frequency link power supplies, power supplies for specialized applications and high-current protection circuits.

Since 1988, he has been with the Department of Electrical and Computer Engineering, University of Toronto, where he is engaged in teaching and research. His areas of research interest include static power converters and their applications, signal processing in power engineering applications, energy storage systems, and device or process modeling. He has also participated as a Consultant or Project Leader in several industrial projects.

Dr. Dawson is a member of the Association of Professional Engineers of Ontario.



Mary Pugh was born in Washington, DC, USA, in 1966. She received the B.A. degree in pure mathematics from the University of California at Berkeley, Berkeley, CA, USA, in 1986, and the M.S. and Ph.D. degrees in mathematics from the University of Chicago, Chicago, IL, USA, in 1988 and 1993, respectively.

From 1993 to 1997, she was a Post-Doctoral Researcher at the Courant Institute and at the Institute for Advanced Study. From 1997 to 2001, she was an Assistant Professor at The University of Pennsylvania, Philadelphia, PA, USA. Since 2001, she has been an Associate Professor at the University of Toronto, Toronto, ON, Canada. Her research is largely on the modeling, analysis, and simulation of thin films of viscous liquids, with a broader interest in computational methods for partial differential equations.



Amgad A. El-Deib (S'02–M'09) received the B.A.Sc. and M.A.Sc. degrees from Cairo University, Cairo, Egypt, in 2002 and 2005, respectively, and the Ph.D. degree from the University of Toronto, Toronto, ON, Canada, in 2010, all in electrical engineering.

From 2002 till 2005, he was a Teaching Assistant in the Electrical Power and Machines Department, Cairo University. He was with the Energy Systems group in the Department of Electrical and Computer Engineering, University of Toronto, as a Research Assistant and a Postdoctoral Fellow until 2012. Currently, he is with Hatch Ltd., Niagara Falls, ON, Canada, working mainly on renewable power projects. His areas of research interest include static power converters, in particular, drivers for discharge lamps and LEDs, coupled physics modeling and numerical solution techniques, and power systems analysis and control. The focus of his research is currently directed toward the modeling and control of renewable power systems incorporating energy storage elements.